ELSEVIER

Effects of ion bombardment on properties of d.c. sputtered superhard (Ti, Si, Al)N nanocomposite coatings

E. Ribeiro[a], A. Malczyk[a,1], S. Carvalho[a], L. Rebouta[a,*], J.V. Fernandes[b], E. Alves[c], A.S. Miranda[d]

[a]*Physics Department, University of Minho, Azurém, 4800-058 Guimarães, Portugal*
[b]*Centro de Engenharia Mecânica — FCT, Universidade de Coimbra, 3030 Coimbra, Portugal*
[c]*Physics Department, ITN, E.N.10, 2686-953 Sacavém, Portugal*
[d]*Mechanical Engineering Department, University of Minho, Azurém, 4800-058 Guimarães, Portugal*

Abstract

A d.c. reactive magnetron sputtering technique was used to deposit (Ti, Si, Al)N films. The ion current density in the substrate was varied by the superimposition of an axially symmetric external magnetic field between the substrate and target. It was found that the variation of the magnetic field strength induced changes in the ion current density in the substrate with a consequent change in film properties. XRD patterns of sputtered films revealed changes of the lattice parameter (from 0.418 nm to approx. 0.429 nm) with the increase of the ion/atom arrival rate ratio. As already reported for samples prepared by r.f. sputtering, both can be assigned to a cubic B1 NaCl structure, typical for TiN. The lowest lattice parameter corresponds to a metastable phase where Si and Al atoms occupy Ti positions, while the highest lattice parameter corresponds to a system where at least a partial segregation of TiN and SiN$_x$ phases already occurred, leading to the formation of a nanocomposite film of the type nc-TiAlN/a-Si$_3$N$_4$. The mixture of the metastable phase with nanocomposite coating phases in some samples indicates that, in general, the segregation of TiN and SiN$_x$ phases is not complete. Hardness values as high as 45 GPa were measured. Small Si additions to (Ti, Al)N coatings induce a reduction in the pin-on-disk sliding wear rate. © 2002 Elsevier Science B.V. All rights reserved.

Keywords: Ti–Al–Si–N; Superhard coatings; Nanocomposites; Mechanical properties; Wear rate

1. Introduction

Recently the study of multiphase materials based on grain refinement has deserved special attention [1–4]. These materials, commonly called nanostructured materials, are defined as materials having a characteristic length scale less than approximately 20 nm. Some of these nanocrystalline materials exhibit unusual mechanical and structural properties, such as, superhardness, enhanced elasticity and thermal stability. The design of these kinds of superhard nanocrystalline composites is associated with the preparation of a composite material consisting of nanocrystallites embedded within a very thin amorphous matrix [3,5,6]. As suggested by Veprek [6], in nanocrystalline materials nanocracks propagate within the thin amorphous matrix and are hindered by nanocrystallites, which limits the size of nanocracks to a few nanometres. Though the structure and size of nanocrystalline grains in the hard phase, as well as, the thickness of the amorphous tissue appears to be the determinant parameters influencing the mechanical properties of the crystalline/amorphous nanocomposite coatings, a large cohesive energy is also necessary at the interfaces in order to decrease the total free energy of the system [7,8].

Examples of these nanostructured materials are the systems consisting of a nanocrystalline transition metal nitride/amorphous Si$_3$N$_4$ composites, nc-Me$_n$N/a-Si$_3$N$_4$, (Me = Ti, W, V,...) which can reach hardness values of 40–60 GPa [9–18] and a high elastic recovery (up to 80%), as well as an enhanced thermal stability (up to 1100 °C) [17], as well the system nc-TiN/a-Si$_3$N$_4$/a- and nc-TiSi$_2$ which revealed an ultrahardness higher than 80 GPa [19]. Ti–B–N coatings also showed high hardness values, which reach a maximum when TiB$_2$ and TiN phases coexist in equal parts [20,21]. Recently, the superhardness revealed by nc-ZrN/Cu [22]

* Corresponding author. Tel.: +351-253510151; fax: +351-253510153.
 E-mail address: rebouta@fisica.uminho.pt (L. Rebouta).
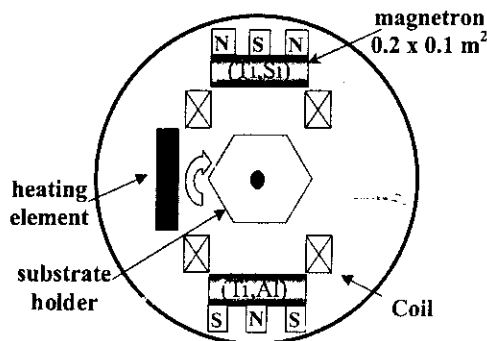 [1] On leave from: Mechanical Technical Engineering Department, Gliwice University, Poland.

Fig. 1. Schematic description of the deposition system.

Fig. 2. Ion and Ti+Al atoms fluxes and ion/atom arrival rate ratio as functions of the magnetic field at the substrate position.

coatings indicated the possibility of a new type of superhard nanocomposite coating, in the form of nc-MeN/metal. Another type of coating, also in the form of a nanocomposite, nc-TiC/a-C [23], also showed high hardness values, but with a remarkable plastic deformation.

The reported results revealed that intense ion bombardment is required to synthesize nc-TiN/a-Si_3N_4 coatings. An important factor in the microstructure of nitride coatings is the ion/atom arrival ratio J_{ion}/J_{atom} [24], which has a significant effect on growth of the nanocrystalline TiN grains. Under low energy ion bombardment the radiation damage in the subsurface region is reduced, while the adatom mobility is enhanced. This is also a way to control not only the hardness, but also the elastic modulus in order to improve the wear resistance.

In this paper (Ti, Si, Al)N coatings deposited on high-speed steel substrates produced by reactive magnetron sputtering were studied. The aim of this study is to understand the mechanical properties evolution as a function of different magnetic fields at substrate position and bias voltages and its correlation with the developed texture.

2. Experimental details

Deposition of (Ti, Si, Al)N samples was carried out in a laboratorial deposition system described in Fig. 1. The system consists of two vertically opposed rectangular magnetrons in a closed field configuration. The magnetron sources are unbalanced of type 2 [25]. The films were deposited in an Ar/N_2 atmosphere by reactive d.c. magnetron sputtering onto polished high-speed steel (AISI M2). A Ti adhesion layer was deposited onto these substrates before coating deposition. The substrates were positioned on a rotating holder (~7 rev./min). The target-to-substrate distance was kept at 70 mm in all runs. A $Ti_{0.5}Al_{0.5}$ target and a Ti target with some incrusted Si pieces were used in the preparation of the (Ti, Si, Al)N samples. An external heating resistance positioned at 80 mm from the substrate holder was used to heat the samples. In static mode and with
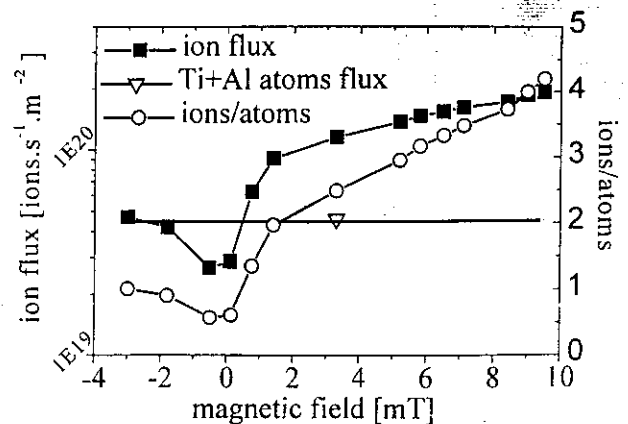
a current density of 10 mA cm^{-2} in the target, the substrate temperature reached 340 °C. During depositions in rotation mode the substrate temperature was not measured, being lower than that obtained in static mode, but strongly dependent on the deposition rate and on the ion-to-atom arrival rate ratio.

Rectangular solenoid coils, made of isolated Cu wire, were placed between the targets and the substrate holder. The external magnetic field created by a d.c. current passing through a coil allowed the variation of the ion flux towards the substrate. When coils were not used, the axial component of the magnetic field in the substrate holder had a value of 3.3 mT. When a 5 A d.c. current passed through the 210 turns of the coil, an external magnetic flux of 9.5 mT was obtained.

We estimated the ion flux (J_{ion}) as being the density saturation bias current [26,27] and the deposition flux (J_{atom}) through the deposition rate including the Ti and Al atoms during the (Ti, Al)N preparation in static mode. In order to evaluate the ion flux at the substrate, the saturation ion current to the substrates was measured using a 2.5 cm in diameter flat steel probe positioned in the substrate holder. The saturation current was measured as a function of the coil current at a constant probe voltage of −150 V. With a current density of 10 mA cm^{-2} in the target and a working gas (Ar/N_2) pressure of 0.45 Pa, the saturation current in the substrate was approximately 1.8 mA cm^{-2}. During (Ti, Al)N deposition the Ti+Al flux, J_{Ti+Al}, was 4.6×10^{19} m^{-2} s^{-1} and the ion/atom arrival ratio fluxes changed continuously from 2.5 (without coils) to approximately 4.2 (with a magnetic field of 9.5 mT in the substrate), as shown in Fig. 2. For the different values of external magnetic field the atom flux was assumed as constant. The floating potential corresponding to these two deposition conditions changed from 24 V to 30 V. The atomic composition of the as-deposited samples was measured by Rutherford backscattering spectrometry

(RBS) and electron microprobe analysis (EMPA). RBS was performed using a He$^+$ beam with energy of 2 MeV and a H$^+$ beam with energy of 1.5 MeV in order to obtain the atomic areal density (atoms cm^{-2}) of the films. Ball cratering tests were used to measure the thickness of the samples. The typical thickness of the films was approximately 2 μm. The density was estimated with the areal atomic density, extracted from RBS measurements, divided by the thickness.

X-Ray diffraction (XRD) experiments were undertaken in a Philips PW 1710 apparatus using Cu K$_\alpha$ radiation, in order to examine film texture and microstructure. The deflection method was used to evaluate the residual stress. Hardness and Young's modulus measurements were performed in a Fisherscope H100, using a maximum load of 40 mN, whose details are reported elsewhere [13]. Pin-on-disk sliding wear tests were performed at room temperature using a Si$_3$N$_4$ pin subjected to a normal force of 5 N. The sliding speed of the disks, with a diameter of 70 mm, was 0.5 m s^{-1}.

3. Results and discussion

3.1. Microstructure, composition and properties of as deposited samples

RBS and EPMA analyses showed that coatings are almost stoichiometric. The composition and density, as well the bias and the magnetic field at substrate position used in the preparation of representative (Ti, Al, Si)N samples are displayed in Table 1. The sample TA was prepared without Si and in static mode. All other samples were prepared in rotation mode, the first three with a current density on magnetrons of 5 mA cm^{-2} and the remaining with a current density of 10 mA cm^{-2}. Although using the same two targets with the same current, the composition varied with the superimposed external magnetic field. The increase in the ion/atom arrival rate ratio induces resputtering in the substrate, with a selective removal of Si. A significant density increase of the films was observed in the presence of the external magnetic field, as a consequence of the increase of low energy ion bombardment.
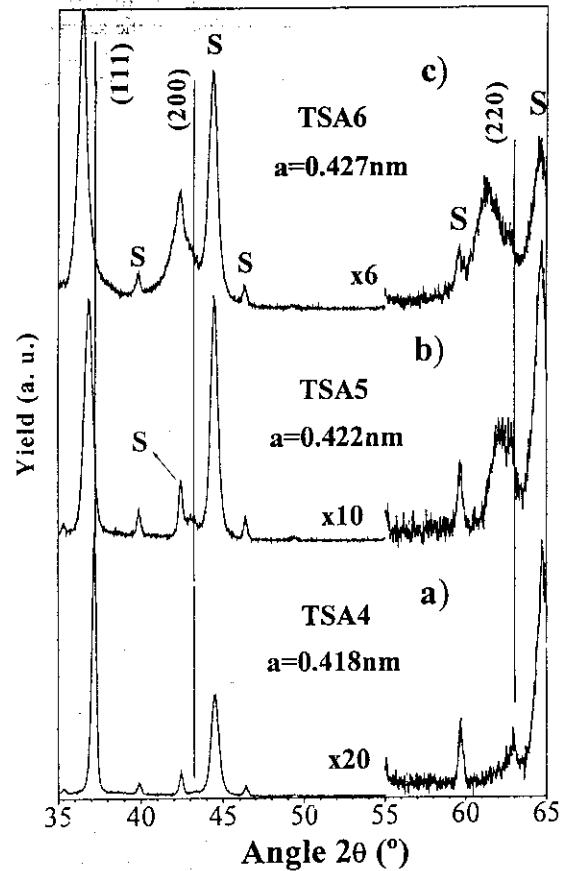

Fig. 3. XRD patterns of (Ti, Al, Si)N samples prepared by d.c. magnetron sputtering in rotation mode corresponding to the samples described in Table 1. The straight lines correspond to peak positions for a lattice parameter of 0.418 nm. The peaks from the substrate are labelled with S.

XRD patterns representative of the general behaviour of the prepared samples are shown in Fig. 3. In this figure are shown patterns of samples prepared with a current density on magnetrons of 10 mA cm^{-2} and a deposition rate of approximately 2.1 μm h^{-1}. The patterns labelled from (a) to (c) correspond to samples prepared with increasing magnetic field at the substrate position, corresponding to an enhanced ion-to-atom arrival rate ratio. The main preferential orientations can be

Table 1

Composition and density of the samples, and bias and magnetic field at the substrate position used during the depositions

Sample	Ti (% at.)	Al (% at.)	Si (% at.)	N (% at.)	Bias (V)	Magnetic field (mT)	Density (g/cm^3)
TA	22.5	27.5	–	50	−50	3.3	3.7
TSA1	32.0	13.1	4.4	50.5	−50	3.3	3.8
TSA2	27.2	13.9	6.4	52.5	−70	7.1	4.2
TSA3	30.0	13.8	4.1	52.1	−70	9.5	4.5
TSA4	26.8	15.1	5.8	52.3	−50	3.3	3.5
TSA5	23.5	15.8	7.7	53.0	−50	7.1	4.6
TSA6	41.1	10.6	2.7	45.6	−70	9.5	4.5

The (Ti, Al)N sample was prepared by static mode and the (Ti, Al, Si)N samples were deposited by rotation mode.

Table 2
Residual stress, hardness and Young's modulus of the samples

Sample	Stress (GPa)	Hardness (GPa)	Young's modulus (GPa)
TA	–	31	480
TSA1	–	17	295
TSA2	−5.1	39	406
TSA3	−7.8	42	400
TSA4	–	30	446
TSA5	−3.8	35	444
TSA6	−5.1	45	491

indexed to a fcc structure, typical for TiN. With the lowest ion-to-atom arrival rate ratio (without coils) a phase with a lattice parameter of 0.418 nm is formed. These conditions associated with low deposition temperature do not provide the necessary atomic surface mobility in the growing film. Thus, neither the phase segregation, nor the consequent formation of the poly-crystalline grains and the amorphous tissue are ensured, as was also observed in samples prepared by r.f. mag-netron sputtering [14,28,29]. The Ti replacement by Si and Al explains the low lattice parameter value for this metastable phase ($\sim$0.418 nm). With the increase in ion/atom arrival rate ratio, when surface mobility is enough, the segregated Si can be sufficient to nucleate and develop the Si_3N_4 phase that forms a layer on the growth surface, covering the (Ti, Al)N nanocrystallites and limiting their growth. The formation of a superhard nc-TiAlN/a-Si_3N_4/a-AlN should be also considered due to the effect of enhanced ion bombardment. This induces a partial Al segregation, with AlN precipitation, as already reported for (Ti, Al)N films [30]. From peak widths in the XRD patterns a grain size decrease is also evident, which is consistent with Si and possibly Al segregation.

3.2. Ultramicrohardness, elastic modulus and pin-on-disk sliding wear

Table 2 presents the compressive residual stress, the hardness and the Young's modulus of the samples described in Table 1. Samples prepared without external magnetic field revealed low hardness values, which is related to low substrate temperature during deposition. The hardness increased substantially with the change of bias and the magnetic field at the substrate position. The increase in surface mobility induced by the enhanced ion-to-atom arrival rate ratio and the corre-sponding increase in substrate temperature are enough to ensure an enhancement in the nanocrystals/amor-phous phase segregation, increasing the hardening ben-efits, as well as film elastic behaviour, that can be ascribed to this structural arrangement. However, as expected the compressive residual stress increases with ion bombardment. The high compressive stress can be

responsible for a hardness enhancement [31]. However, it is not the hardness value alone to determine the coating applicability, as shown in Fig. 4, where are displayed the hardness and elastic modulus, as well as the pin-on-disk sliding wear rate against a Si_3N_4 pin, for the samples TA, TSA5 and TSA6. Data are reported also for three (Ti, Al, Si)N samples prepared by r.f. sputtering (sample 7 and 8) and by a combination of r.f. and d.c. supplying (sample 9) and for another (Ti, Al)N sample, also prepared by r.f. sputtering (sample TA-r.f.). The latter four samples were included, due to their high hardness and Young's moduli and microstruc-ture [32]. The microstructure of these samples has some similarities with those of former samples, where the sample 8 has the same texture of sample 6 and the microstructure of samples 5 and 9 is also similar.

A first analysis of Fig. 4 suggests that only in certain cases the incorporation of Si resulted in a coating that showed a reduced sliding wear. The better performance of sample TSA6 (sliding wear rate of 1×10^{-14} m^2 N^{-1}) is related to the high ion/atom arrival rate ratio used during deposition. The low Si content, a lower grain size associated with lattice parameter and super-hardness suggest a nanostructure of the type nc-TiAlN/a-Si_3N_4/a-AlN. The higher density is also a parameter usually associated with better mechanical performance. Similar behaviour was revealed by sample 8 ($Ti_{0.69}Si_{0.15}Al_{0.16}N$) [29,32], that evidenced an analo-
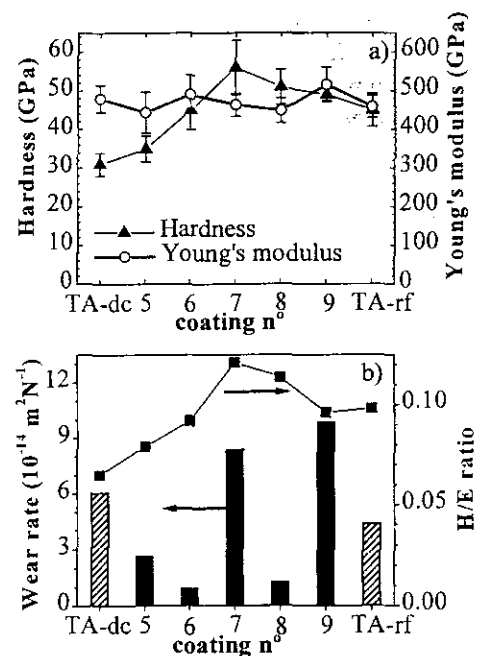

Fig. 4. (a) Correlation between the measured hardness and the Young's modulus of the (Ti, Al, Si)N samples and (b) respective pin-on-disk sliding wear rates against a Si_3N_4 pin, and ratio between hard-ness and elastic modulus. The (Ti, Al)N samples are represented by patterned bars.

gous XRD pattern, although prepared by r.f. sputtering. XRD patterns of sample 9 ($Ti_{0.66}Si_{0.13}Al_{0.21}N$), as well as of sample TSA5, revealed a lattice parameter slightly lower than that of TiN, which suggests the development of the metastable phase where Ti atoms are replaced by Si and Al atoms. The intermediate lattice parameter values can be explained by the relatively high residual stresses and by an incomplete segregation of TiN and SiN_x phases; this leads to a possible mixture of TiN grains and regions constituted by the so called solid solution. Among the two, TSA5 revealed better wear rate, but also evidenced the mentioned mixture, although being the softer sample.

Some studies have suggested that the ratio between hardness and elastic modulus H/E plays an important role to the coating performance [33]. Although the statistics are not relevant, the wear behaviour and the corresponding H/E values of samples presented in Fig. 4 are not conclusive. Not only a high hardness determines the wear behaviour. In this study samples with similar H/E ratio revealed distinct sliding wear rate, suggesting that in multiphase nanocomposites the microstructure plays an important role.

In general, the (Ti, Al, Si)N samples revealed friction coefficients slightly lower than those of (Ti, Al)N samples (~0.85), the best result being a friction coefficient of 0.7.

4. Conclusions

XRD results suggest the following phase composition of the (Ti, Al, Si)N films, depending on the adopted deposition parameters:

- a cubic phase with lattice parameter of approximately 0.418 nm, that corresponds to a metastable phase (Ti, Al, Si)N, where Si and Al atoms occupy Ti positions;
- a system where at least a segregation of TiAlN and SiN_x phases already occurred, leading to the formation of a nanocomposite film of the type nc-TiAlN/a-Si_3N_4 and possibly nc-TiAlN/a-Si_3N_4/a-AlN;
- a mixture of the metastable phase and nanocomposite coating phases, indicating that, in general, the segregation of TiN and SiN_x phases is not complete.

The low deposition temperature and the reduced ion bombardment induce low species mobility in the growing film that cannot efficiently segregate the nanocrystalline/amorphous phase type structure. Increasing ion bombardment and temperature results in an enhancement of mechanical properties. These benefits are particularly visible in hardness values, where an increase in ion bombardment (increase in coil current) corresponds to a hardness increase from 30 to 45 GPa, as well as on the wear resistance where a decrease on sliding wear rate from 6×10^{-14} m^2 N^{-1} to 1×10^{-14} m^2 N^{-1} was observed.

References

[1] M. Nastasi, D.M. Parkin, H. Gleiter (Eds.), Mechanical properties and deformation behaviour of materials having ultra-fine microstructures, NATO ASI Series, vol. 233, Kluwer Academic Publ, Dordrecht, 1993.

[2] A.S. Edelstein, R.C. Cammarata (Eds.), Nanomaterials: Synthesys, Properties and Applications, Institute of Physics Publ, Bristol, 1996.

[3] S. Veprek, Crit. Rev. J. Vac. Sci. Technol. A17 (1999) 2401.

[4] J. Musil, Surf. Coat. Technol. 125 (2000) 322.

[5] H. Gleiter, Prog. Mater. Sci. 33 (1989) 223.

[6] S. Veprek, Thin Solid Films 317 (1998) 449.

[7] H. Gleiter, in: M. Nastasi, D.M. Parkin, H. Gleiter (Eds.), Mechanical properties and deformation behaviour of materials having ultra-fine microstructures, NATO ASI Series, vol. 233, Kluwer Academic Publ, Dordrecht, 1993, pp. 3–35.

[8] A. Niederhofer, P. Nesládek, H.D. Männling, S. Veprek, M. Jílek, Surf. Coat. Technol. 120/21 (1999) 173.

[9] T. Hirai, S. Hayashi, J. Mater. Sci. 17 (1982) 1320.

[10] J.S. Reid, X. Sun, E. Kolawa, M.A. Nicolet, IEEE Electron. Device Lett. 15 (1994) 298.

[11] L. Shizhi, S. Yulong, P. Hongrui, Plasma Chem. Plasma Process. 12 (1992) 287.

[12] S. Veprek, S. Reiprich, Thin Solid Films 268 (1995) 64.

[13] F. Vaz, L. Rebouta, S. Ramos, M.F. da Silva, J.C. Soares, Surf. Coat. Technol. 108/109 (1998) 236.

[14] F. Vaz, L. Rebouta, B. Almeida, et al., Surf. Coat. Technol. 120/121 (1999) 166.

[15] P. Holubár, M. Jílek, M. Sima, Surf. Coat. Technol. 120/21 (1999) 184.

[16] C. Louro, A. Cavaleiro, Surf. Coat. Technol. 123 (2000) 192.

[17] S. Veprek, P. Nesládek, A. Niederhofer, F. Glatz, M. Jílek, M. Šíma, Surf. Coat. Technol. 108/109 (1998) 138.

[18] M. Diserens, J. Patscheider, F. Lévy, Surf. Coat. Technol. 120/121 (1999) 158.

[19] S. Veprek, A. Niederhofer, K. Moto, et al., Surf. Coat. Technol. 133/134 (2000) 152.

[20] P. Hammer, A. Steiner, R. Villa, et al., Surf. Coat. Technol. 68/69 (1994) 194.

[21] C. Mitterer, P.H. Mayrhofer, M. Beschliesser, et al., Surf. Coat. Technol. 120/121 (1999) 405.

[22] J. Musil, P. Zeman, H. Hrubý, P.H. Mayrhofer, Surf. Coat. Technol. 120/121 (1999) 179.

[23] A.A. Voevodin, S.V. Prasad, S. Zabinski, J. Appl. Phys. Lett. 82 (1997) 855.

[24] L. Hultman, W.-D. Munz, J. Musil, S. Kadlec, I. Petrov, J.E. Greene, J. Vac. Sci. Technol. A 9 (1991) 434.

[25] B. Window, N. Savvides, J. Vac. Sci. Technol. A 4 (1986) 196.

[26] I. Ivanov, P. Kazansky, L. Hultman, I. Petrov, J.-E. Sundgren, J. Vac. Sci. Technol. A 12 (1994) 314.

[27] P.J. Kelly, R.D. Arnell, J. Vac. Sci. Technol. A 16 (1998) 2858.

[28] F. Vaz, L. Rebouta, P. Godeau, et al., Surf. Coat. Technol. 133/ 134 (2000) 307.

[29] S. Carvalho, F. Vaz, L. Rebouta, D. Schneider, A. Cavaleiro, E. Alves, Surf. Coat. Technol. 142/144 (2001) 110.

[30] J. Musil, H. Hrubý, Thin Solid Films 365 (2000) 104.

[31] L. Karlsson, L. Hultman, J.-E. Sundgren, Thin Solid Films 371 (2000) 167.

[32] S. Carvalho, L. Rebouta, A. Cavaleiro, L.A. Rocha, J.Gomes, E. Alves, Surf. Coat. Technol., in print.

[33] A. Leyland, A. Matthews, Wear 246 (2000) 1.